Neural desynchronization and arousal differentially shape brain states for optimal sensory performance

Leonhard Waschke*, Sarah Tune, & Jonas Obleser*
University of Lübeck, Germany

*Author correspondence:
Leonhard Waschke, Jonas Obleser
Department of Psychology
University of Lübeck
Maria-Goeppert Straße 9a
23562 Lübeck
Email: leonhard.waschke@uni-luebeck.de, jonas.obleser@uni-luebeck.de

Number of words in Abstract: 152
Number of words in Introduction: 816
Number of words in Discussion: 2420

Keywords: Arousal, Desynchronization, Perceptual decision-making, Noradrenaline, Entropy, EEG

Conflict of interest: The authors declare no competing financial interests.

Author contributions: LW and JO designed research. LW recorded data. LW analysed data with contributions from JO and ST. LW, ST, and JO wrote the manuscript.

Acknowledgments: Research was supported by the European Research Council (ERC Consolidator grant 646696 to JO) and a G.A. Lienert foundation scholarship (LW). Franziska Scharata, Philip Seidel, and Simon Grosnick helped acquire the data. We thank Hong-Viet V. Ngo for help with illustrations, Björn Herrmann for help with source projection, Santiago Jaramillo for helpful comments on an earlier version of this manuscript, and three reviewers for their constructive feedback.

Abstract

Instantaneous brain states have consequences for our sensation, perception, and behaviour. Both fluctuations in arousal and in neural desynchronization likely pose perceptually relevant states. However, their relationship and their relative impact on perception is unclear. We here provide evidence that, at the single-trial level in humans, desynchronization in sensory cortex (expressed as time-series entropy) and pupil-linked arousal differentially impact perceptual processing. While we recorded electroencephalography (EEG) and pupillometry data, stimuli of a demanding auditory discrimination task were presented into states of high or low desynchronization of auditory cortex via a real-time closed-loop setup. Desynchronization and arousal distinctly influenced stimulus-evoked activity and shaped behaviour displaying an inverted u-shaped relationship: States of intermediate desynchronization elicited minimal response bias and fastest responses, while states of intermediate arousal gave rise to highest response sensitivity. Our results speak to a model in which independent states of global arousal and local desynchronization jointly optimise sensory processing and performance.

Introduction

The way we sense and perceive our environment is not determined by physical input through the senses alone. The dynamics of ongoing brain activity affect the build-up of sensory representations and our conscious perception of the physical world. Recently, instantaneous fluctuations of both pupil-linked arousal[1–3] and neural desynchronization[4–6] have been highlighted as sources of such sensory and perceptual variations: Arousal and cortical desynchronization are two ways of characterizing the brain state, which strongly influences sensory cortical responses, the encoding of information, thus perception and ultimately behaviour.

Pupil-linked arousal, which likely captures locus coeruleus-norepinephrine activity (LC–NE; ref. [7–9]) has been shown to influence sensory evoked activity[2,10,11] and the processing of task-relevant information[1,12]. Despite evidence for an inverted u-shaped relation of LC–NE activity to performance long suspected from the Yerkes-Dodson law[13], the precise associations between arousal, sensory processing, and behaviour are underspecified: Although optimal performance at intermediate levels of arousal has reliably been observed[2,11,12,14,15], reports of linear effects on performance[10] or evoked activity[16] in different tasks and species complicate this picture.

In a separate line of experimental work in non-human animals, relatively high neural desynchronization yielded improved encoding and representation of visual[17–19] as well as auditory input[5,6,20]. Such periods of desynchronization are characterized by reduced noise correlations in population activity, and these patterns are commonly referred to as desynchronized cortical states. They likely result from subtle changes in the balance of excitatory and inhibitory activity[21,22]. Although desynchronization and perceptual performance are positively linked in general[17,23], the exact shape of their relationship (linear vs. quadratic) is unclear. Most notably, evidence for a similar mechanism in humans has remained elusive.

At first glance paradoxically, a tight link of pupil size and desynchronization has been claimed[11,24], while both measures have also been found to be locally unrelated[17,25]. As of now, pupil-linked arousal and cortical desynchronization may or may not be distinct signatures of the same underlying process: Varying noradrenergic and cholinergic activity could influence both, local cortical activity and the more global measure of pupil size via afferent projections from brain-stem nuclei[26]. In sum, it is, first, unclear how pupil-linked arousal and cortical desynchronization precisely shape sensory processing and perceptual performance in humans. Second, the interrelation of both measures and their potentially shared underlying formative process lacks specification.

Here, we set out to test the relationship of desynchronized cortical states and pupil-linked arousal, and to specify their relative impact on sensory processing and perception in healthy human participants. We recorded EEG and pupillometry while participants performed a challenging auditory discrimination task. A closed-loop real-time algorithm calculated on-line an information theoretic proxy of cortical desynchronization (weighted permutation entropy, WPE, refs. [27,28]) based on EEG signal arising predominantly from auditory cortices. Of note, WPE as a proxy of desynchronization is tailored to the analysis of electrophysiological time series: It captures oscillatory as well as non-oscillatory contributions as a time-resolved estimate of desynchronization (see methods for details). Importantly, EEG entropy calculated for

a previously published data set[29] aptly tracks changes in excitatory and inhibitory (E/I) cortical activity that occur under different anaesthetics (Figure S1). Also, EEG entropy as measured in the present data aligns closely with the spectral exponent[30], a previously suggested measure of E/I.

We used this measure of ongoing desynchronization to trigger stimulus presentation during relatively synchronized and desynchronized states, respectively. A continuously adapting criterion enabled us to effectively sample the whole desynchronization state space[31]. Such a closed-loop set up allows for selective stimulation during specific states of brain activity while accounting for changes in the appearance of those states and hence represents a powerful tool with a multitude of potential applications in research but also therapy[32,33]. To evaluate the interrelation of pre-stimulus desynchronization with simultaneously acquired pupil-linked arousal as well as their influence on stimulus-related activity we employed linear mixed-effect models. Furthermore, psychophysical models were used to evaluate the impact of desynchronization and arousal on perceptual sensitivity, response criterion, and response speed.

Although cortical desynchronization and pupil-linked arousal were weakly positively correlated, both did not only shape the ongoing EEG activity into distinct states, but also differentially influenced sensory processing at the level of single trials: Phase-locked activity in low frequencies as well as stimulus-related gamma power over auditory cortices was highest following intermediate levels of pre-stimulus desynchronization. On the other hand, induced low-frequency power during and after a stimulus increased linearly with pre-stimulus arousal. Response criterion and speed exhibited an inverted u-shaped relationship with cortical desynchronization, that is, intermediate desynchronization corresponded to minimal response bias and fastest responses. An analogous relationship was found for arousal and sensitivity, revealing highest sensitivity at intermediate arousal levels.

Our results speak to a model in which global arousal states and local desynchronization states jointly influence sensory processing and performance. While fluctuations in arousal are likely realized by afferent cholinergic and noradrenergic projections into sensory cortical areas[34,35], desynchronization states on the other hand might result from efferent feedback connections.

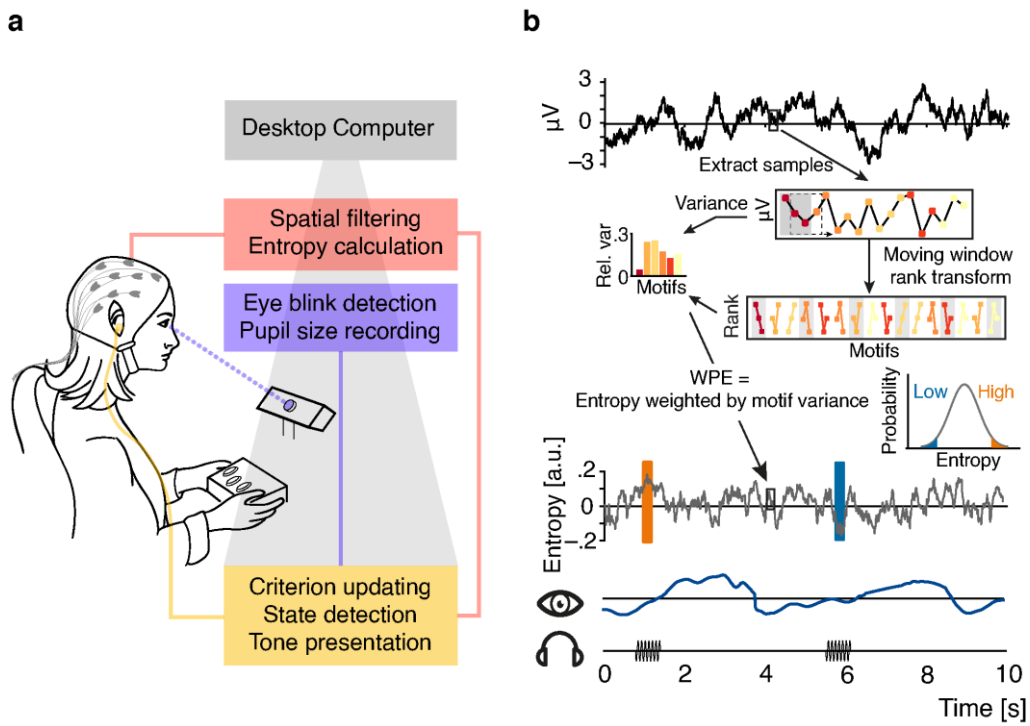

Figure 1. Illustration of the real-time closed-loop setup to track states of desynchronization (**A**) Setup: EEG signal was spatially filtered before entropy calculation. Pupil size was recorded and monitored consistently. Pure tone stimuli were presented via in-ear headphones during states of high or low entropy of the incoming EEG signal. (**B**) Schematic representation of the real-time algorithm: spatially filtered EEG signal (one virtual channel) was loaded before entropy was calculated using a moving window approach (illustrated for 18 samples in the upper box; 200 samples were used in the real-time algorithm). Voltage values were transformed into rank sequences ("motifs") separated by one sample (lower box; Eq. 1 in Methods; different colors denote different motifs), and motif occurrence frequencies were weighted by the variance of the original EEG data constituting each occurrence (equation 3 & 4). Each entropy value was calculated based on the resulting conditional probabilities of 200 samples, before the window was moved 10 samples forward (i.e., effectively down-sampling to 100 Hz). Inset: The resulting entropy time-course was used to build a continuously updated distribution (forgetting window = 30 s). Ten consecutive entropy samples higher than 90% (or lower than 10%) of the currently considered distribution of samples defined states of relatively high and low desynchronization, respectively. Additionally, pupil size was sampled continuously.

Results

We recorded EEG and pupillometry while participants (n = 25; 19–31 years old) performed an auditory pitch discrimination task. On each trial participants were presented with one tone, taken from a set of seven pure tones (increasing pitch from tone 1 through tone 7), and had to decide whether that tone was rather high or low in pitch with regard to the overall set of tones. Participants thus compared each tone to an implicit standard, the median (= mean) pitch of the set. This yielded in all participants a valid psychometric function mapping stimulus pitch to perceptual decisions (see Fig. S5).

Critically, by means of a real-time closed-loop algorithm (see Fig. 1), tones were presented during states of relatively high or low entropy of auditory cortical EEG, a proxy of cortical desynchronization. By collapsing offline across the whole experiment, we obtained data that covered the whole range of desynchronization states occurring in a given participant[31]. We then combined (generalized) linear mixed-effects models and psychophysical modelling to test the effects of cortical desynchronization as well as pupil-linked arousal on (1) ongoing as well as sensory-related EEG activity, and on (2) perceptual performance.

Real-time closed-loop algorithm dissociates desynchronization states

Entropy of EEG signals emerging from auditory cortices was calculated with the help of an established, localizer-based spatial filter (see Fig. 2A; refs.[36,37]) and a custom real-time algorithm (Fig. 1). Source projection of localizer data which were used to construct the subject-specific spatial filters revealed predominantly auditory cortical regions as generators (Fig. 2A).

Note that the distribution of entropy values which provided the basis for the classification of relatively high vs. relatively low desynchronization states was updated continuously, with two crucial consequences: First, this approach minimized the potential impact of slow drifts in desynchronization on brain state classification. Second, the continuously updated criterion allowed us to, effectively, sample the whole state space of desynchronization states: Depending on the current distribution, the same absolute entropy value could be classified as a high state, for example in the beginning of the experiment, and as a low state half an hour later. This focus on local, short-lived states resulted in widely overlapping pre-stimulus entropy distributions of high and low states (Fig. 2C) which were then used as continuous predictor alongside the equally continuous pupil-size in all subsequent analyses.

Demonstrating the performance of the real-time algorithm, average entropy time-courses were elevated for all classified-high compared to all classified-low states in a 200 ms pre-stimulus window (all $P < .001$, FDR corrected; Fig. 2B). Note that this result is non-trivial. Since we continuously updated the criterion for state detection, in theory, states classified online as high and low could have yielded the same average entropy across the entire experiment.

In contrast, pupil diameter time-courses did not differ between high and low entropy states at any point in time (all $P > .1$) nor did the distributions of pre-stimulus pupil diameters (Fig. 2C). In line with previous research[38], pupil size and entropy in the pre-stimulus time window were positively related ($\beta = .02$, SE = .01, $P = .02$). Pupil size explained less than 1% of the variance in EEG entropy.

Most relevant to all further analyses, we conclude that states of cortical desynchronization in auditory cortex and pupil-linked arousal predominantly occurred independently of each other.

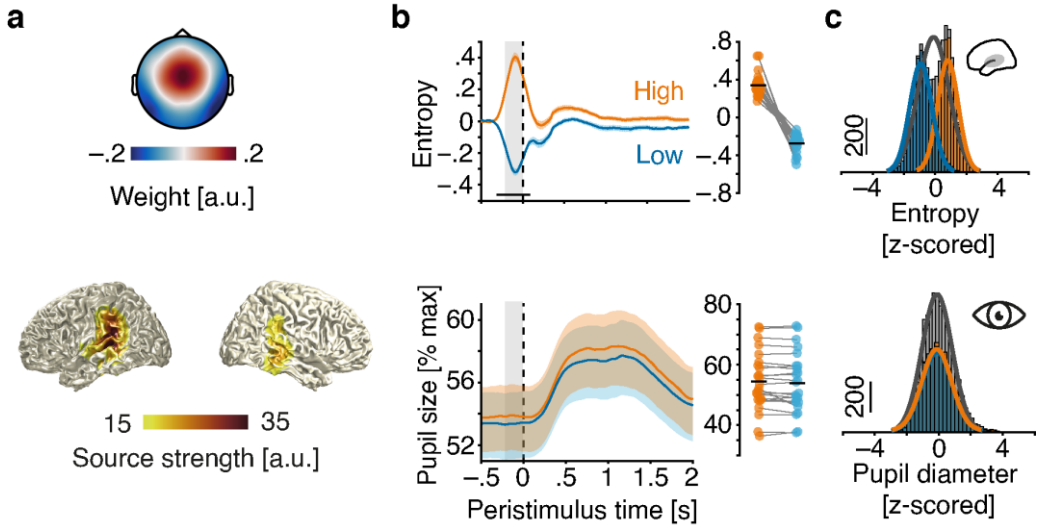

Figure 2. Evaluation of the real-time closed-loop setup for states of desynchronization and arousal (**A**) Grand average spatial filter weights based on data from an auditory localizer task (top) and grand average source projection of the same data (masked at 70% of maximum; bottom). (**B**) Grand average time-courses of entropy (upper panel) and pupil diameter (lower panel) for low-entropy (blue) and high-entropy states (orange) ± standard error of the mean (SEM). Subject-wise averages in the pre-stimulus time-window (-200–0 ms, grey boxes) in right panels. Entropy was logit transformed and baseline corrected to the average of the preceding 3 seconds. Pupil size was expressed as percentage of each participant's maximum pupil diameter across all pre-stimulus time-windows. (**C**) Histograms and fitted distributions of z-scored pre-stimulus entropy (top) and z-scored pupil size (bottom) for low-entropy states (blue), high-entropy states (orange), and both states combined (grey). Note the independence of entropy states and pupil states.

Cortical desynchronization and pupil-linked arousal pose distinct states of ongoing activity

To dissociate the corollaries of cortical desynchronization and pupil-linked arousal on ongoing EEG activity, we modelled single trial pre-stimulus oscillatory power over auditory cortical areas as a function of pre-stimulus entropy and pupil diameter by jointly including them as predictors in linear mixed-effects models. Of note, non-baselined values of EEG entropy and pupil size were used as predictors but baseline values of EEG entropy were included as covariates to control for the influence of slow temporal drifts. All analyses of ongoing or stimulus-related EEG activity were carried out on the spatially filtered EEG signal, allowing us to concentrate on brain activity dominated by auditory cortical regions.

As expected based on the definition of entropy and earlier results[28], these analyses revealed a negative relationship of entropy and oscillatory power within the pre-stimulus time window (-200–0 ms; see Fig. 3). With increasing pre-stimulus entropy, low-frequency pre-stimulus power decreased (1–8 Hz, $\beta = -.19$, SE = .01, $P < .001$; table S1). Gamma power (40–70 Hz) also decreased, although to a lesser degree ($\beta = -.16$, SE = .01, $P < .001$; table S2). Gamma power was lowest at intermediate entropy levels (quadratic effect; $\beta = .05$, SE = .01, $P < .001$). Auditory EEG entropy hence aptly approximates the degree of auditory cortical desynchronization.

Conversely, and underscoring a distinction of both measures, pupil size was associated with an increase in pre-stimulus low-frequency power (1–8 Hz, β = .02, SE = .01, *P* = .1) and a decrease in gamma power (40–70 Hz, β = -.03, SE = .01, *P* = .005; see Fig. 3). The distinct effect of EEG entropy and pupil size on low-frequency power was additionally supported by a Wald test (Z_{Wald} = 13.8, *P* > .001). Put differently, in these stimulus-free periods in auditory cortex, low-frequency power was low given strong desynchronization, while it was high given large pupil-linked arousal. Notably, both patterns of results did not hinge on the exact choice of frequency ranges.

High desynchronization states were thus characterized by reduced oscillatory broad-band power overall, while high arousal states were accompanied by an increase in low-frequency power and a decrease in higher-frequency power.

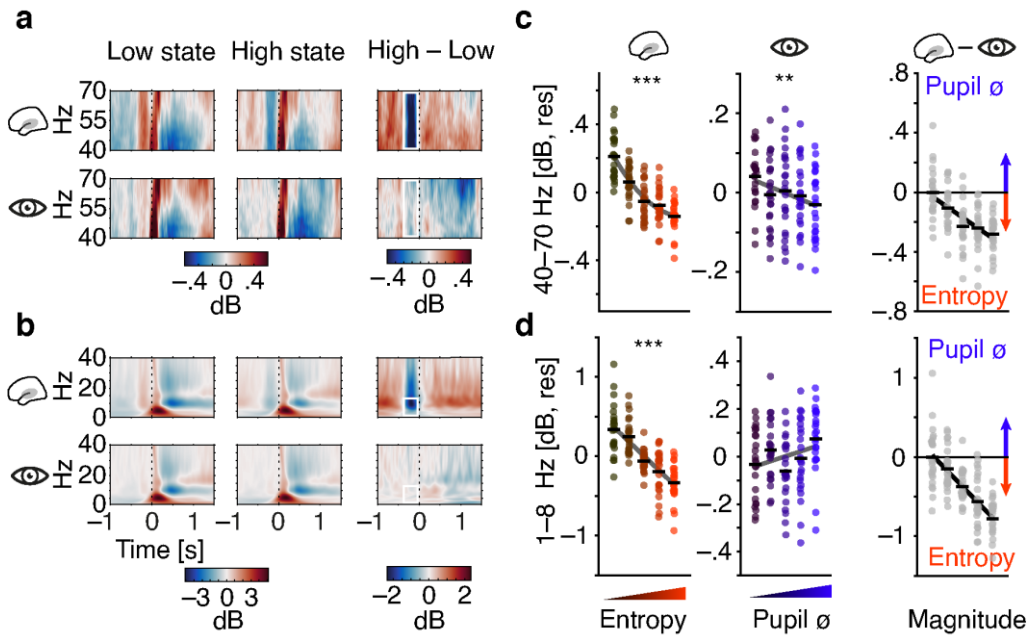

Figure 3. Impact of pre-stimulus entropy and pupil size on ongoing auditory cortical EEG activity. (**A**) Grand average gamma power across time (40–70 Hz, baselined to -1–0 s, in dB) for low states (left), high states (middle) and the difference of both (right). Entropy states shown in the upper, pupil states in the lower panel. Dashed line represents tone onset, white rectangle outlines the pre-stimulus window of interest. (**B**) As in (A) but for 0–40 Hz. (**C**) Mean-centred single subject (dots) and grand average gamma power (black lines) in the pre-stimulus time-window (-.4–0 s, white rectangle), residualized for pre-stimulus baseline and pupil size, shown for five bins of increasing pre-stimulus entropy (left) and pupil size (residualized for entropy baseline and pre-stimulus entropy, middle). Grey line represents average fit, red colours show increasing entropy, blue colours increasing pupil size. Effects of entropy and pupil size are contrasted in the right panel. (**D**) As in (C) but for low-frequency power (1–8 Hz). Note the different y-axis range between entropy and pupil effects. All binning for illustrational purposes only. ***P < .001, **P < .01

Differential effects of desynchronization and pupil-linked arousal on auditory evoked activity

Next, to investigate the influence of those pre-stimulus states on sensory processing, we tested the impact of cortical desynchronization and pupil-linked arousal in this pre-stimulus time window on auditory, stimulus-evoked EEG activity. Analogous to the procedure outlined above, we used linear mixed-effects models to estimate the effects of entropy and pupil size on sensory evoked power and phase coherence over auditory cortices. Note that we modelled continuous variables instead of an artificial division into high vs. low states. While low-frequency phase coherence quantifies how precise in time neural responses to stimuli appeared across trials, low-frequency power captures the magnitude of evoked responses regardless of their polarity[39,40]. In addition, high frequency power after stimulus onset likely originates from sensory regions and depicts sensory processing[41]. If EEG entropy and pupil size entail perceptual relevance they should also influence sensory processing as approximated by the outlined measures. Please note that all measures of sensory processing were based on artefact-free EEG data.

First, we found low-frequency single-trial phase coherence after stimulus onset, a measure quantifying the consistency of phase-locked responses on a trial-wise basis (see Methods for details), to increase with pre-stimulus entropy (1–8 Hz, 0–400 ms; $\beta = .05$, SE = .01, $P < .001$, Fig. 4A, D). Additionally, phase coherence was highest following intermediate levels of pre-stimulus entropy, as evidenced by a negative quadratic effect ($\beta = -.02$ SE = .009, $P = .02$).

Of note, there was no comparable relationship of pupil size and single-trial phase coherence (1–jITC, see methods for details; $\beta = -.00001$, SE = .00004, $P = .8$; $Z_{Wald} = 1.5$, $P = .1$; table S3). Phase-locked responses hence increased with pre-stimulus cortical desynchronization but were unaffected by variations in arousal.

Second, we observed a linear increase of low-frequency power after stimulus onset, a common proxy of stimulus-induced activity, as a function of pre-stimulus pupil size (1–8 Hz, 0–400 ms; $\beta = .05$, SE = .01, $P < .001$, Fig. 4B, E). In contrast, pre-stimulus entropy did not affect post-stimulus power ($\beta = .002$, SE = .011, $P = .9$; table S4). Therefore, stimulus-induced activity increased with arousal but remained unaltered under changing levels of cortical desynchronization ($Z_{Wald} = 3.2$, $P = .001$).

Third, we detected linearly increasing post-stimulus gamma power, representing early auditory evoked activity, with rising pre-stimulus entropy (40–70 Hz, 0–400 ms; $\beta = .07$, SE = .01, $P < .001$, Fig. 4C, F). Furthermore, as evidenced by a negative quadratic relationship, stimulus-related gamma power was maximal when stimuli were presented during intermediate entropy states ($\beta = -.02$, SE = .009, $P = .02$). Conversely, post-stimulus gamma power decreased with growing pre-stimulus pupil size ($\beta = -.02$, SE = .01, $P = .06$; table S5). Auditory evoked gamma power hence was inversely influenced by two different measures of brain state: while it increased with cortical desynchronization, it decreased with growing arousal ($Z_{Wald} = 2.7$, $P = .007$). Notably, neither desynchronization nor pupil size had any effect on the tone-evoked activity when expressed as event-related potentials (see Fig. S1).

Overall, single-trial auditory sensory evoked activity was differentially influenced by desynchronization and arousal. While only higher desynchronization was associated with increased phase-locked responses, only arousal was positively

linked to stimulus-induced activity. In addition, with desynchronization showing a positive and arousal a negative link to stimulus-evoked gamma power, both measures exert opposite influences on the early processing of auditory information.

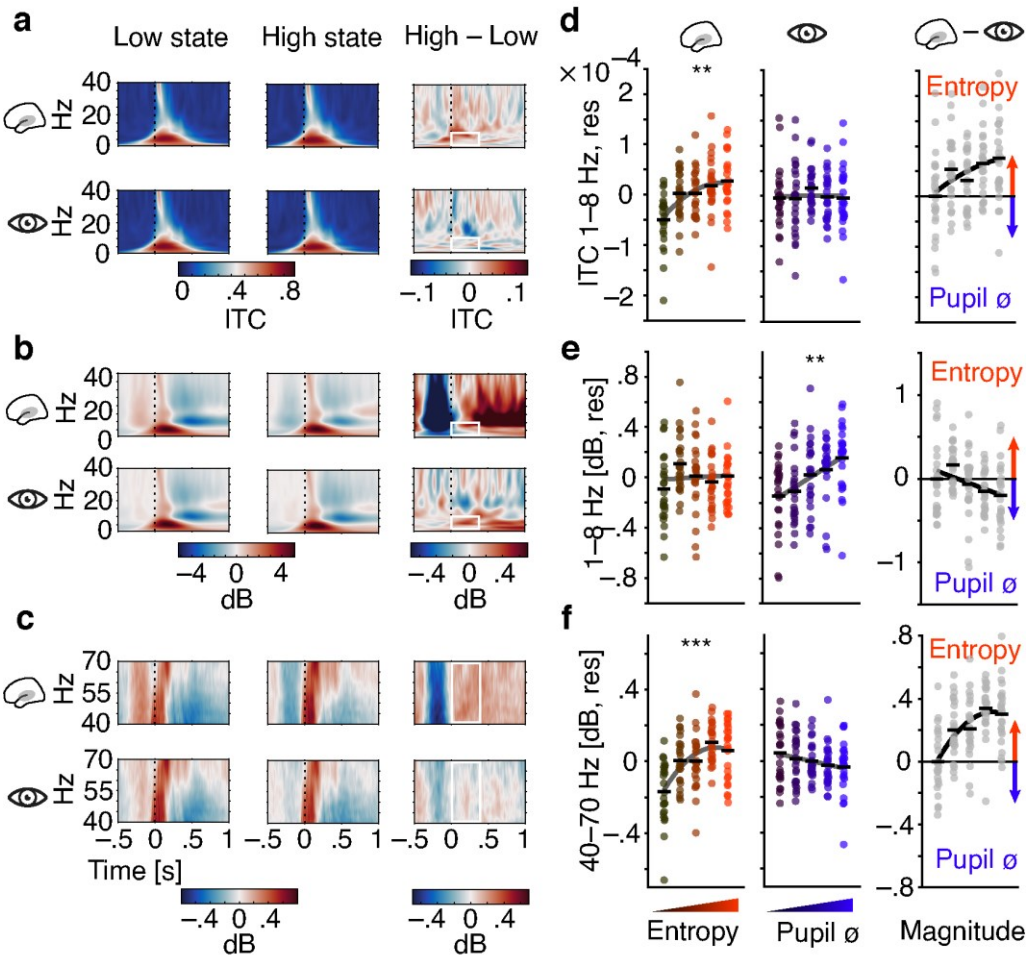

Figure 4. Influence of pre-stimulus entropy and pupil size on tone-related activity. (**A**) Grand average ITC (0–40 Hz) across time for low states (left), high states (middle) and the difference of both (right). Entropy states shown in the upper, pupil states in the lower panel. Dashed black lines indicate tone onset, white rectangles the post-stimulus window of interest. (**B**) As in (A) but for low-frequency power (0–40 Hz, baselined to -1–0 s). (**C**) As in (B) but for gamma power (40–70 Hz). (**D**) Mean centred single subject (dots) and grand average ITC (black lines), residualized for baseline entropy and pupil size, in the post-stimulus time-window (0–.4 s, 1–8 Hz) for five bins of increasing pre-stimulus entropy (left) and pupil size (residualized for entropy baseline and pre-stimulus entropy, middle). Grey line represents average fit, red colours increasing entropy, blue colours increasing pupil size. Effects of entropy and pupil size are contrasted in the right panel. (**E**) As in (D) but for post-stimulus low-frequency power (0–.4 s, 1–8 Hz). (**F**) As in (E) but for post-stimulus gamma power (0–.4 s, 40–70 Hz). Again, all binning for illustrational purposes only. ***$P < .001$

Desynchronization and arousal differently impact perceptual performance

To examine the impact of desynchronization and arousal on perceptual performance, we modelled binary response behaviour ("high" vs. "low") as a function of stimulus pitch, pre-stimulus desynchronization, and arousal using generalized linear mixed-

effects models (see *Statistical analyses* for details). In brief, this statistical approach describes binary choice behaviour across the set of used tones and thus also yields a psychometric function, but the generalized linear framework allows us to include the neural predictors of interest. Two parameters of the resulting functions were of interest to the current study: (1) the threshold of the psychometric function represents the response criterion; (2) the slope of the psychometric expresses perceptual sensitivity. Additionally, we tested the influence of desynchronization and arousal on response speed (i.e., the inverse of response time, in s^{-1}).

Participants were least biased and answered fastest at intermediate levels of pre-stimulus desynchronization: pre-stimulus entropy displayed a negative quadratic relationship with response criterion (log odds (log OR) = -.06, SE = .02, P = .02; Fig. 5A, table S6) and response speed (β = -.012, SE = .004, P = .002; Fig.5 C, table S7). A reduced model that allowed the inclusion of single-subject effects as random slopes revealed that this negative quadratic effect of entropy on response criterion was observable in all participants (see Fig. 5 A). Average predicted response times were lowest following intermediate pre-stimulus entropy (.716 s) compared to low (.762 s) and high (.786 s) entropy. States of intermediate neural desynchronization hence led to a reduction in response time of 50-60 ms compared to high and low desynchronization states.

On the other hand, participants proved most sensitive at intermediate levels of arousal: pupil size exhibited negative linear as well as quadratic relations with sensitivity (linear: log OR = -.232, SE = .068, P = .001; quadratic: log OR = -.153, SE = -.035, P < .001; table S6) but not with response speed (β = -.004, SE = .003, P = .1; Fig. 5 D, table S7). As above, a model including random slopes resulted in negative effects for the vast majority of participants (see Fig. 5 B). Highest sensitivity hence coincided with intermediate arousal and decreased from there.

Like pre-stimulus entropy, pupil size did covary with response criterion. However, the relationship was linearly decreasing (high arousal coincided with a decreased criterion; log OR = -.115, SE = .028, P < .001; Fig 5 C, table S6) and lacked the marked quadratic relationship observed for pre-stimulus entropy (cf. Fig. 5A). The increase in bias with arousal was clearly driven by states of particularly high arousal.

To directly compare the relative impact of EEG entropy and pupil size on behaviour, respectively, we computed a Wald statistic (Z_{Wald}) for each dependent behavioural measure. The Wald statistic puts the difference between two estimates from the same model in relation to the standard error of their difference. The resulting Z value can be used to test against equality of the two estimates. While response criterion was predicted by EEG entropy following an inverted U shape but not by pupil size (Z_{Wald} = –2.9, P = .004), response speed was predominantly influenced by pre-stimulus entropy (Z_{Wald} = –1.94, P = .05). Conversely, pupil size predicted sensitivity better than EEG entropy (Z_{Wald} = 1.6, P = .1).

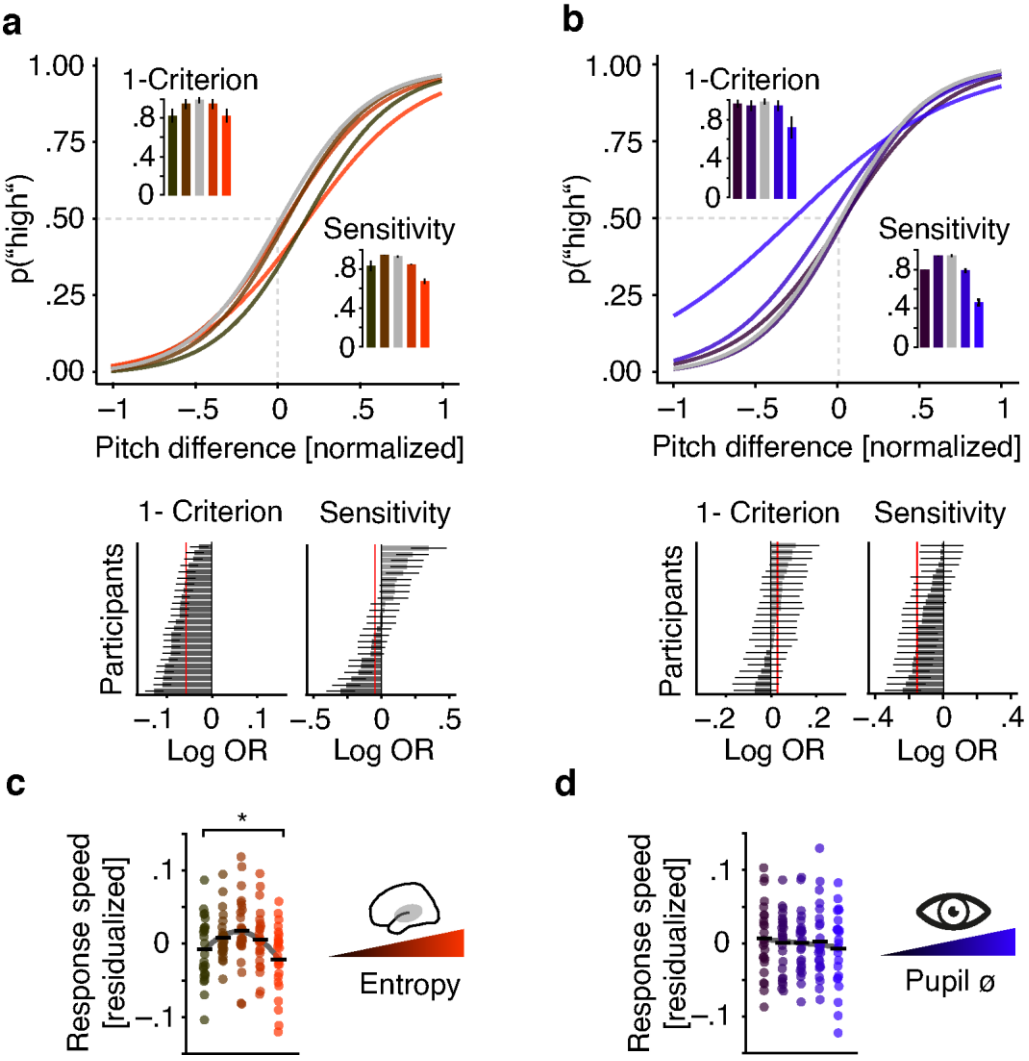

Figure 5. Effects of pre-stimulus entropy and pre-stimulus pupil size on perceptual performance. (**A**) Fixed effects results: probability of judging one tone as "high" as a function of pitch difference from the median (normalized), resulting in grand average psychometric functions for five bins of increasing entropy (red colours). Dashed grey lines indicate bias-free response criterion. Insets show 1–criterion (upper) and sensitivity estimates (lower) including SEMs. Bottom left panel shows single subject log odds (log OR) for the quadratic relationship of pre-stimulus entropy and response criterion (± 95 % CI), bottom right panel single subject log ORs for the quadratic relationship between pre-stimulus entropy and sensitivity. Participants sorted for log OR, red line marks fixed effect estimate. (**B**) As in (A) but for five bins of increasing pre-stimulus pupil size. (**C**) Single subject (dots) and average response speed (black lines) as a function of increasing pre-stimulus entropy (five bins). (**D**) As in (C) but as a function of pre-stimulus pupil size. Again, all binning for illustration only. * $P < .005$

Control analyses

Pre-stimulus oscillatory power in auditory cortex does not predict behavioural outcome in the auditory discrimination task.

The substantial negative correlation of desynchronization states quantified by entropy on the one hand and low-frequency oscillatory power on the other (see Fig. 3; refs. [5,28]) prompted us to repeat the modelling of perceptual performance with pre-stimulus power instead of entropy as a predictor. If entropy only represents the inverse of oscillatory power, effects should remain comparable but change their sign. Oscillatory power however was not significantly linked to behaviour (all $P > .15$) and including power as an additional predictor in the model of performance outlined above did not explain additional variance (model comparison, $\chi^2(1) = .7$, $P = .40$). Thus, cortical desynchronization but not oscillatory power was linked to perceptual performance.

Visuo-occipital entropy does not predict behavioural outcome in the auditory discrimination task.

To test the cortico-spatial specificity of the outlined desynchronization states to the auditory domain, we repeated all analyses of stimulus-evoked activity and behaviour based on entropy as calculated from visuo-occipital channels. Specifically, we replaced auditory entropy with visual entropy before re-running all relevant models (see Methods for details).

Unsurprisingly, as these spatial filter weights yield imperfect renderings of local cortical activity, we observed a sizable correlation between this visuo-occipital entropy signal and the auditory entropy signal central to our analyses ($\beta = .40$, SE = .009, $P < .001$). However, since visual and auditory entropy were also sufficiently distinct (shared variance only $R^2 = 15$ %), more detailed analysed on their specific effects were warranted.

We first regressed this visuo-occipital entropy signal on pupil size and observed a weak negative relationship ($\beta = -.02$, SE = .009, $P = .03$). Relationships of pre-stimulus entropy over visual cortex with stimulus-evoked auditory activity generally displayed the same direction as for auditory cortex entropy (see Fig. 6A for summary). Adding to the domain specificity of our main findings, however, visual cortex entropy was a markedly weaker predictor of single-trial phase coherence (model comparison compared to a model with auditory entropy; Bayes factor (BF_{A-V}) = 18,319), low-frequency power (BF_{A-V} = 21,669), and gamma power (BF_{A-V} = 34,634; see Fig. 6).

Furthermore, visual cortex entropy showed no relationship with response criterion (log OR = .009, SE = .02, $P = .66$; table S8). Visual cortex entropy had no effect on response speed ($\beta = -.002$, SE = .003, $P = .5$) and auditory cortex entropy explained response time data better (BF_{A-V} = 10.7). The influence of pre-stimulus desynchronization on stimulus processing and behaviour thus proves to be local in nature, and most selective to desynchronization in sensory regions that are involved in the current task.

Discussion

This study tested the influence of cortical desynchronization and pupil-linked arousal on sensory processing and perceptual performance. We recorded EEG and pupillometry, while stimuli of a demanding auditory discrimination task were selectively presented during states of high or low desynchronization in auditory cortex. Cortical desynchronization and arousal differentially affected ongoing EEG activity and had distinct effects on stimulus-related responses. Furthermore, at the level of single trials, we find unbiased performance and highest response speed to coincide with intermediate levels of pre-stimulus desynchronization and highest sensitivity following intermediate levels of arousal.

Tracking of auditory cortical desynchronization in real-time

As revealed by the average spatial filter and source projection (Fig. 2), the signal central to the present analyses mainly originated from auditory cortical areas. The state-detection algorithm we employed was based on entropy of the spatially filtered EEG signal and performed the desired state-dependent presentation with sufficient precision in time (Fig. 2 B). Of note, the distribution used to classify desynchronization states in real-time was updated constantly, which ensured two central prerequisites: First, slow drifts in desynchronization over time were prevented from biasing the state classification. Second, we were able to sample, throughout the experiment, the whole desynchronization state space within each participant[31]. In contrast to an algorithm that sets the criterion for state classification only once per participant and leaves it unchanged thereafter ("open-loop"), the current approach can be referred to as a closed-loop. Technical advances have promoted the use of such closed-loop paradigms to various areas of neuroscientific research, where the main application lies in neurofeedback. Neurofeedback tries to modify behavior by providing participants with sensory information that is directly proportional to their current brain state[14,33]. Just recently, a number of methodically sophisticated studies have used the power of this approach to relate fluctuations in working memory[32] or decision making[42] to brain activity in real-time.

Cortical desynchronization and arousal differentially shape states of ongoing EEG activity

While there was a pronounced difference in EEG entropy between states of high and low desynchronization, illustrating the power of the used real-time algorithm, no such difference was found for the time-course of pupil size (Fig. 2). Although pupil size and EEG entropy were positively correlated as has been reported before[38], a major part of the variance in EEG entropy was not accounted for by pupil size. We take this as a first piece of evidence that two distinct mechanisms are involved in the generation of perceptually relevant brain states.

Furthermore, changing degrees of desynchronization and arousal manifested in diverse ways in the ongoing EEG: On the one hand, desynchronization in the pre-stimulus time window was negatively related to concurrently measured oscillatory power over a wide range of frequencies (Fig. 3). The strong negative relationship with low-frequency power replicates previous findings[28] and is tightly linked to the concept of entropy[28]. On the other hand, pupil-linked arousal in the same time window was positively linked to low-frequency power, an association frequently observed in invasive recordings of non-human animals[2,24]. Additionally, arousal was

negatively related to high-frequency power. This negative link of arousal and gamma power differs from reports of a positive relationship between gamma power of local field potentials (LFP) and pupil size[24]. Of note, Vinck and colleagues (2015) correlated pupil diameter and LFP gamma power over time within an event-locked time period. In contrast, we related the average pupil diameter in a pre-stimulus time window to spontaneous EEG gamma power across trials. Differing methods might be the reason for the seeming disparity of effects.

Taken together, the distinct relationships that desynchronization and arousal entertain with key, frequency-domain metrics of instantaneous EEG activity emphasize their independence. We take this as additional evidence for two distinct mechanisms of origin.

Neurophysiological and neuromodulatory processes of desynchronization and arousal

How plausible is this idea of at least two, at least partially segregate drivers of perceptually relevant brain state? LC–NE activity has been proposed to reflect changes in arousal captured by variations in pupil size[7]. Although fluctuations in pupil size have recently been linked to activity in the superior colliculus or the ventral tegmental area[43] and also carry information about cholinergic activity[9], converging evidence suggests a tight connection to LC-NE activity [7–9,43]. At the same time, in addition to adrenergic and cholinergic projections from brain-stem nuclei, glutamatergic cortico-cortical and thalamo-cortical feedback connections have been proposed as a source of varying states of desynchronization[26]. The widespread NE projections from LC[7] are a likely cause for the demonstrable effects of NE-linked arousal on sensory encoding in both the auditory[11] as well as visual domain[24]. This rationale would thus predict that arousal states should not differ substantially between different sensory cortical regions.

However, modulatory effects of arousal have been found to depend on the experimental context as well as on the sensory modality[44,45]. The weak correlation of desynchronization and arousal might thus trace back to our focus on auditory cortical areas. An imperfect direct arousal–desynchronization link in the present data becomes more plausible if we take into account the important distinction between global and local brain states: While the overall level of arousal should have widespread but modality- and context-specific impact on sensory processing and behaviour[2,7], the desynchronization of local sensory neural populations could be largely unrelated to, and take place on top of, those global changes[17].

Such rather local and modality-specific changes in desynchronization have been assumed to arise from both thalamo- and cortico-cortical feedback connections that represent the allocation of selective attention[26,46,47]. More precisely, glutamatergic projections between thalamus, prefrontal, and sensory cortical areas might shape the local net degree of inhibition in populations of sensory neurons via AMPA and NMDA receptors and hence influence time-varying local desynchronization. In fact, contingent on the specific task structure, selective attention increases desynchronization in neurons with stimulus-related receptive fields but also across a broader range of task-relevant neurons[48,49]. In keeping with this, desynchronization over auditory but not visual cortical areas predicted sensory processing and performance (Fig. 6). A next step would thus be to combine the

present setup for desynchronization–dependent stimulation with manipulations of selective attention.

All things considered, the involvement of two partially related mechanisms in the concomitant generation of desynchronization and arousal states appears likely. On the one hand, desynchronization states presumably are shaped by feedback connections that could result from fluctuations in selective attention. On the other hand, pupil-linked arousal states at least partially hinge on varying levels of LC–NE activity[8,9] which are propagated via vast projections towards most regions of cortex and which might be related to overall changes in the availability of cognitive resources.

If cortical desynchronization and arousal indeed originate from two distinct processes that both entail functional and behavioural relevance, they should not only have differential effects on the processing of sensory information but also on perceptual performance — which is what we observed here, as discussed next.

Sensory processing is distinctly affected by desynchronization and arousal states

Desynchronized cortical states have previously been associated in the rodent with enhanced encoding of auditory stimuli[5], more reliable neural responses[6], and improved perceptual performance[17]. Instead, when optogenetically inducing synchronization, perception is impaired[50]. Arousal on the other hand has been linked to increased sensory processing of visual stimuli in mice[16] and humans[10]. However, perceptual performance was found to be highest at either intermediate[11,16] or maximum arousal levels[10].

In the current study, desynchronization and arousal had clearly dissociable effects on sensory processing and behaviour at the single-trial level. First, phase locked responses and stimulus-related gamma power were strongest following intermediate levels of pre-stimulus desynchronization (Fig. 4). Strikingly, those relationships of desynchronization and sensory processing were mimicked by perceptual performance: Intermediate desynchronization led to optimal response criterion and response speed, hence yielding minimally biased and fastest performance (Fig. 5). Second, increased levels of arousal were linked to a rise in stimulus-related low-frequency power, and intermediate arousal levels yielded maximum sensitivity.

Of note, the described tri-fold association of desynchronization, stimulus-evoked activity, and response criterion is generally in accordance with a number of recent studies researching the influence of pre-stimulus oscillatory power on perceptual decisions. Generally, pre-stimulus power in the EEG has been found to bias choice behaviour[51]. More specifically, however, alpha power (8–12 Hz) prior to stimulus onset has been tightly linked to changes in response criterion and confidence[52–54]. Pre-stimulus alpha power is hypothesized to represent changes in baseline excitability, linking it to response criterion following an inverted u-shaped relationship[55,56]. These previous findings and the here reported connection of desynchronization and response criterion might at least partially trace back to the same underlying mechanism: that is, task- and attention-specific input to sensory cortical regions via efferent projections leading to a change in net inhibition.

572 Furthermore, although both our present measures of brain state were
573 positively associated with stimulus-related EEG activity, they affected phase-locked
574 and non-phase-locked brain responses as well as behaviour in distinct ways (see
575 Figure 6A). Be reminded, however, that all effects on behaviour and stimulus-related
576 activity were not obtainable when replacing auditory entropy with measures of
577 auditory oscillatory power or with visuo–occiptial entropy instead, which underlines
578 their specificity.

579 Effectively, desynchronization and arousal might interact separately with the
580 two, long-debated building blocks of sensory evoked responses: phase resetting of
581 low-frequency oscillations and additive low-frequency activity[57,58]. The positive link
582 between phase-locked responses and desynchronization replicates previous findings
583 from our group[28] and, combined with the observation of maximum phase coherence
584 as well as stimulus-related gamma power following intermediate desynchronization,
585 indicates enhanced early processing of auditory information. Tones presented into
586 states of intermediate desynchronization thus led to a stronger phase-reset.

587 By contrast, states of pre-stimulus high arousal intensified stimulus-induced,
588 low-frequency activity. While phase-locked responses to a stimulus are believed to
589 represent primarily thalamo–cortical or bottom-up activity and early sensory
590 processing, stimulus-induced activity has been hypothesized to index primarily
591 cortico–cortical or top-down processes that originate from feedback connections[59].
592 Although the current experimental design does not allow a direct assessment of this
593 interpretation, previous research suggests that stronger phase-locking signals clearer
594 early sensory representations and that increased induced activity points to a more
595 precise integration of sensory information into a reference frame[60,61]. Accordingly,
596 intermediate cortical desynchronization might improve the representation of sensory
597 signals, while arousal could foster the integration of sensory information into such an
598 existing reference frame.

599

600 *Cortical desynchronization and pupil-linked arousal differentially impact performance*

601 Importantly, the dissociation in neural sensory processing parallels a dissociation in
602 behaviour. First, and analogous to the precision of sensory encoding which was
603 highest at intermediate desynchronization levels, responses were least biased
604 following intermediate desynchronization states. This striking parallel in neural and
605 behavioural results cautiously suggests a change in the precision of representations
606 that depends on the current desynchronization state. Second, the impact of arousal
607 on post-stimulus low-frequency power and perceptual sensitivity, in the light of
608 earlier interpretations[60] proposes a similar mechanism: in addition to a clearer early
609 representation of sensory information, intermediate arousal might optimize the
610 integration of such a representation into an existing reference frame. This integration
611 likely involves cortico-cortical feedback connections[59] and is essential to allow
612 sensitive perceptual decisions. A different experimental design that allows the direct
613 investigation of the proposed mechanisms represents a crucial next step to
614 understanding the specific functioning of perceptually relevant brain states on the
615 level on sensory neurons.

616 However, the relationship of arousal and perceptual performance takes a
617 different shape than the respective link to sensory evoked activity might have

suggested. While sensory evoked activity increased monotonically with arousal, sensitivity was highest at intermediate levels of arousal, testimony to the classic Yerkes–Dodson law. It is possible that we did not sample the state space of pupil-linked arousal in its entirety and hence ended up with a distribution that only captures the lower half of an underlying inverted u[14], resulting in a positive linear relationship between pupil-linked arousal and post-stimulus low-frequency power. The effect of arousal on sensitivity that follows an inverted u-shape however, suggests that we sampled the whole range of arousal states.

Additionally, a number of previous observations do in fact match this seeming disarray of stimulus-related activity (increasing monotonically with arousal) and ideal performance (depending quadratically on arousal). First, relatively highest levels of responsiveness in auditory cortical neurons overall can entail the loss of response specificity crucial for precise encoding and perception[62]. Second, and in line with this rationale, over-amplified responses to auditory stimuli have been linked to age-related decreases of cortical inhibition[36]. States of high arousal could thus in principle lead to a similar process of over-amplification and hence prove detrimental to sensory encoding and perception. Third, a recent experiment researching the impact of arousal on visual processing in mice yielded a highly similar pattern of results[16]. Neske & McCormick (2018) highlight the role of noradrenergic projections which might transmit task-related activity most efficiently at intermediate arousal levels[7].

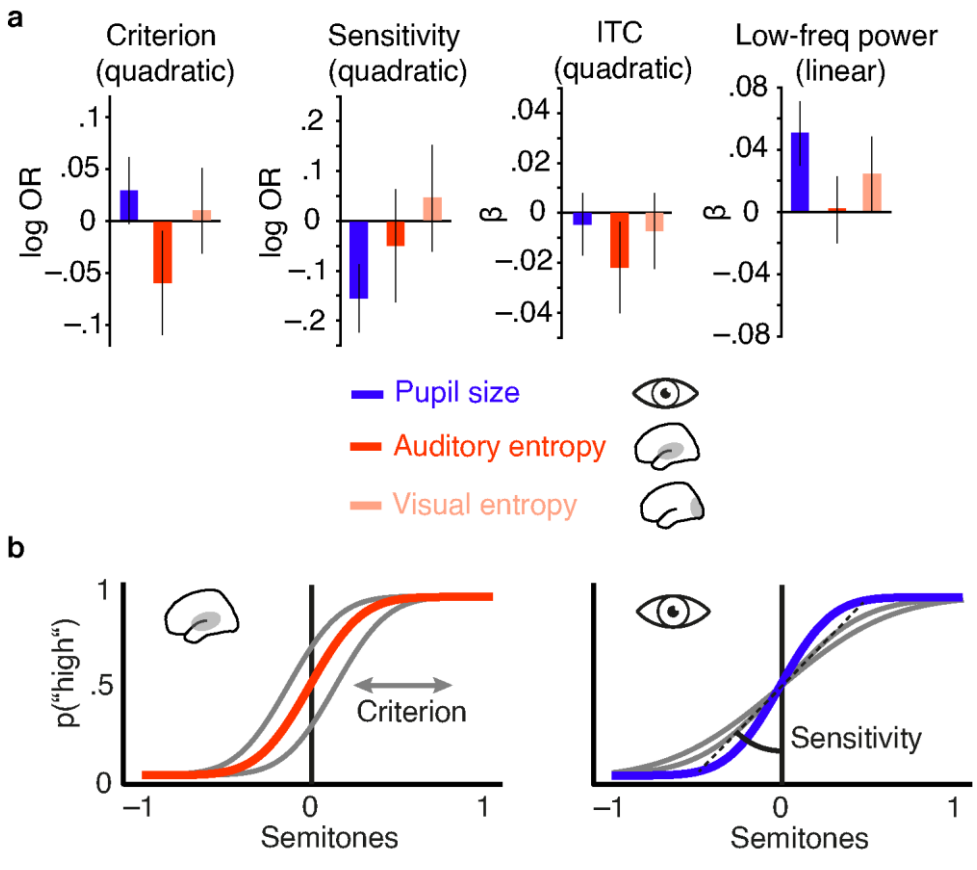

Figure 6. Distinct effects of local desynchronization (i.e., auditory entropy) and global arousal (i.e., pupil size) (**A**) Effect sizes (fixed effects, with 95-% confidence intervals) for the quadratic relationships of criterion and sensitivity with pupil size (blue), auditory cortex entropy (red) and visual cortex entropy (pale pink). Similarly for the quadratic relationship of pupil size, auditory cortex entropy, and visual cortex entropy with ITC and linear relationships with stimulus-related low-frequency power. (**B**) Illustrating the quadratic influence of entropy on response criterion (left panel) and pupil size on sensitivity (right panel) by means of an optimal psychometric function (red vs. blue) and non-optimal ones (grey).

Two interrelated systems of local and global brain state jointly shape perception

We here have presented evidence for a joint role of cortical desynchronization and arousal in the formation of brain states optimal for perceptual performance. The data are commensurate with a model where, on the one hand, arousal shapes global brain states via afferent noradrenergic projections and predominantly influences sensitivity. On the other hand, we see cortical desynchronization in task-related sensory areas to generate local states via attention-dependent feedback connections and to impact response criterion and speed.

To facilitate future research and offer testable hypotheses we intend to leave the reader with some speculations: How could those two mechanisms find an implementation in populations of task-involved sensory neurons? It has been suggested that the shared variability of neuronal populations and its impact on the responses of single neurons are shaped by an additive and a multiplicative source of variation in neural gain[63,64]. Whereas a multiplicative gain factor would lead to an

overall change in tuning width, an additive factor could create an offset which is believed to differ between neurons[65]. Instantaneous fluctuations of cortical activity, or cortical desynchronization, are believed to have an additive effect on evoked responses[63]. Furthermore, LC–NE activity exerts a multiplicative influence on the tuning of sensory neurons, leading to relatively sharper tuning during periods of arousal[66]. It is unlikely that either additive or multiplicative factors alone are the sole source of variability in stimulus-related activity and behaviour[65]. However, the present data allow the testable prediction that selective attention and desynchronization primarily exert an additive influence on neural gain, while LC–NE activity and arousal impact neural gain in a multiplicative fashion.

In sum, the present data provide evidence that, at the single-trial level in humans, desynchronization in sensory cortex (expressed as EEG entropy) and pupil-linked arousal differentially impact sensory and perceptual processes, but jointly optimise sensory processing and performance.

Materials and Methods

Participants: 25 participants (19–31 years, mean age 24.6 years, ± 3.5 years SD; 10 male) with self-reported normal hearing took part in the experiment. Participants gave written informed consent and were financially compensated. None of the participants reported a history of neurological or otological disease. The study was approved by the local ethics committee of the University of Lübeck and all experimental procedures were carried out in accordance with the registered protocol.

Stimulus material: Sets of seven pure tones (±3 steps around 1 kHz; step sizes determined individually, 100 ms duration, 10 ms rise and fall times, sampled at 44.1 kHz) for the main experiment and an additional set of 7 pure tones for the auditory localizer task were created using custom Matlab® code (R2017a; MathWorks, Inc., Natick, MA). Initial stimulus frequencies consisted of six steps (±0.27, ±0.2, and ±0.14 semitones) around the median frequency (1 kHz) but were adjusted during an individual tracking procedure described below. Stimuli were presented via air conducting in-ear head phones (EARTONE 3A), Psychtoolbox and a low latency audio card (RME Audio). All stimuli were presented perfectly audible at a comfortable loudness level approximating 60 dB SPL.

General procedure: Participants were seated in a quiet room in front of a computer screen. First, they completed an auditory localizer task. Second, participants practiced the main task where, in every trial, they compared one tone against the set of seven tones regarding its pitch and difficulty was adjusted to keep performance at approximately 75 % correct. Finally, participants performed 10 blocks of pitch discrimination against an implicit standard (the median pitch, 1 kHz) while tone presentation was triggered by the detection of high or low desynchronization states as outlined below.

Auditory localizer task: Participants listened to 350 pure tones (6 standards, range, 1000–1025 Hz; one oddball at 1050 Hz) separated by inter-stimulus intervals (ISIs) between 1 s and 1.4 s (uniformly distributed). Their task was to detect and count high pitch oddballs (1050 Hz, 50 tones). No overt responses were given during the uninterrupted presentation of tones.

Main experiment: During each trial, participants were presented with one tone out of the same set of seven pure tones (range 1000–1025 Hz) and had to decide whether the presented tone was either high or low in pitch with regard to the whole set of stimuli. In other words, participants implicitly compared each incoming tone to the median frequency in the tone set (i.e., 1000 Hz; Johnson, 1949). To hold task difficulty comparable across individuals, up to four rounds of individual tracking (50 trials each) were carried out where the width of the pitch distribution was adjusted depending on performance after each round. Precisely, the width of the pitch distribution was increased (or decreased) if percentage correct was below 70 % (or above 80 %, respectively). The set of stimuli used during the last round of the tracking procedure was also used during the main experiment.

Pitch discrimination task: Participants were asked to indicate after each tone whether it was high or low in pitch relative to the whole set of stimuli by pressing one of two buttons of a response box (The Black Box Toolkit). Button orientation was reversed for 13 out of 25 participants. They were instructed to answer as fast and as accurate

as possible as soon as the tone had vanished and the response screen had appeared. No feedback was given regarding their performance. A grey fixation cross was presented in the middle of the screen throughout the whole experiment which flickered for one second if participants failed to give a response within 2 seconds after stimulus offset. Participants performed 60 trials per stimulus levels, resulting in 420 trials split up into 10 blocks of 42 trials each. Every block comprised 6 repetitions of each stimulus level in random order. Note that since the exact time point of stimulus presentation was determined depending on current brain states as identified by the real-time approach outlined below, the average tone-to-tone interval varied between individuals (9.14 ± 1.04 s; min = 8.28 s, max = 12.32 s). Visual presentation and recording of responses was controlled by Psychtoolbox.

Data recording and streaming: While participants were seated in a dimly lit, sound attenuated booth, EEG signals were measured with a 64-channel active electrode system (actichamp, BrainProducts, Germany). Electrodes were arranged according to the international 10-20 system and impedances were kept below 10 kΩ. Data were sampled at 1kHz, referenced to electrode TP9 (left mastoid), and recorded using Labrecorder software, part of the Lab Streaming Layer (LSL[68]), also used to create a stream of EEG data, accessible in real-time.

Additionally, eye blinks were monitored and pupil size was recorded by tracking participants' right eye at 500 Hz (Eyelink 1000, SR Research). Pupil data was recorded using Eyelink software on a separate machine but at the same time streamed via a TCP/IP connection to the personal computer that was used for EEG recording, brain-state classification, and stimulus presentation. All recorded data was thus available on one machine.

Spatial filtering and source localization: To focus on EEG activity from auditory cortices, a spatial filter was calculated based on the data from the auditory localizer task of each participant excluding oddball trials. After re-referencing to the average off all channels, we applied singular value decomposition based on the difference between a signal covariance matrix (estimated on EEG data from 0–200 ms peristimulus) and a noise covariance matrix (-200–0 ms peristimulus). This approach resulted in a 64x64 matrix of eigenvalues and the elements of the first eigenvector were used as filter weights (for similar approaches see refs. [37,69]). Matrix multiplication of incoming EEG signals with the spatial filter weights resulted in one virtual EEG channel which largely reflected activity from auditory cortical regions.

To validate this approach, we source localized the same EEG data that was used to construct the signal covariance matrix. To this end, lead fields were computed based on a boundary element method (BEM) template and default electrode locations. Routines from the fieldtrip toolbox[70] and custom code were used to calculate the sLORETA inverse solution[71] which was projected on to the pial surface of a standard structural template (MNI). Arbitrary source strength values were masked at 70 % of the maximum.

Entropy calculation: We computed weighted permutation entropy (WPE) of spatially filtered EEG-signals in a moving window fashion. WPE is an extension to permutation

entropy (PE) which was first developed by Bandt and Pompe (2002)[72] that considers the amplitude fluctuations of time-series data[27] and its calculation is outlined below.

In short, WPE approximates the complexity or desynchronization of any neural time-series via three steps: First, recorded samples (here: microvolts) are transformed into symbolic patterns of a predefined length and distance (equation 1). Second, the probability of occurrence of those patterns within a snippet of data is used to calculate one entropy value[72]. Finally, the amplitude information which is lost during the mapping into symbolic space is partially reintroduced by weighing each patterns probability of occurrence by the relative variance of its corresponding neural data (equations 3 & 4)[27].

In detail, consider the time-series $\{\boldsymbol{xt}\}_{\boldsymbol{t=1}}^{\boldsymbol{T}}$ and a representation incorporating its time delayed sampling $\boldsymbol{X_j^{m,T}} = \left\{\boldsymbol{x_j}, \boldsymbol{x_{j+\tau}}, \dots, \boldsymbol{x_{j+(m-1)\tau}}\right\}$ for $\boldsymbol{j = 1, 2, \dots, T - (m-1)\tau}$ where $\boldsymbol{m}$ is the so called "motif length" and $\boldsymbol{\tau}$ its "time delay factor". The use of both results in a subdivision of the time series into $\boldsymbol{N = T - (m - 1)\tau}$ sub-vectors. Each of those $\boldsymbol{N}$ sub-vectors is mapped into symbolic space by replacing every element, with its rank in the respective sub-vector. Note that the number of possible motifs is limited by the motif length $\boldsymbol{m}$ and amounts to $\boldsymbol{m}!$. The probability of occurrence for all possible motifs $\{\boldsymbol{\pi_i^{m,T}}\}_{\boldsymbol{i=1}}^{\boldsymbol{m!}}$ called $\boldsymbol{\eth}$, which additionally is weighted by $\mathbf{w_j}$, can be defined as:

$$\boldsymbol{p_w(\pi_i^{m,\tau})} = \frac{\sum_{\boldsymbol{j \le N}} \boldsymbol{1_{u:type(u)=\pi_i}(X_j^{m,\tau}).w_j}}{\sum_{\boldsymbol{j \le N}} \boldsymbol{1_{u:type(u)=\in \eth}\left(X_j^{m,\tau}\right).w_j}} \tag{1}$$

Note that ***type*** represents the mapping into symbolic space. Let us furthermore and for simplicity express the weighted occurrence probability of motifs as $\boldsymbol{P_w} = \boldsymbol{p_w(\pi_i^{m,\tau})}$. The weighting of probabilities with weight $\boldsymbol{w_j}$ is achieved by calculating the variance of sub-vectors. Therefore we define the arithmetic mean of $\boldsymbol{X_j^{m,\tau}}$ as:

$$\bar{\mathrm{X}}_{\boldsymbol{j}}^{\boldsymbol{m,\tau}} = \frac{\boldsymbol{1}}{\boldsymbol{m}} \sum_{\boldsymbol{k=1}}^{\boldsymbol{m}} (\boldsymbol{x_{j+(k+1)\tau}}) \tag{2}$$

Each weight value hence is represented by:

$$\boldsymbol{w_j} = \frac{\boldsymbol{1}}{\boldsymbol{m}} \sum_{\boldsymbol{k=1}}^{\boldsymbol{m}} (\boldsymbol{x_{j+(k-1)\tau}} - \bar{\mathrm{X}}_{\boldsymbol{j}}^{\boldsymbol{m,\tau}})^{\boldsymbol{2}} \tag{3}$$

We can finally compute WPE as the Shannon entropy of:

$$\boldsymbol{H(m,\tau)} = -\sum_{\boldsymbol{i:\pi_i^{m,\tau} \in \eth}} \boldsymbol{P_w \log P_w} \tag{4}$$

Since the exact choice of pattern length and distance influences the final entropy estimate we relied on recommendations from modelling work and earlier practice[28,73] by setting the pattern length to 3 and the distance to 1 (number of samples). To ensure approximation acuity but retain a high time-resolution, a 200-samples window was moved along the EEG signal in steps of 10 samples, resulting in an entropy sampling rate of 100 Hz.

Real-time brain-state classification and stimulus triggering: Neural desynchronization in auditory cortical regions was estimated by reading in the EEG signal into Matlab®, re-referencing to the average of all channels, applying the individual spatial filter and calculating a time-resolved version of WPE.

The resulting entropy time-series was used to generate online a distribution of entropy values. Importantly, this distribution was updated constantly such that it never contained values older than 30 seconds. This way, changes in neural desynchronization on longer time-scales were excluded and, instead of a strictly bimodal distribution, the whole state space was sampled and trials presented at essentially all levels of absolute desynchronization were obtained (see Figure 2). Desynchronization states were defined as a minimum of 10 consecutive entropy samples (100 ms) higher or lower than 90% of the current distribution and we will refer to them as high and low states, respectively, in the following.

Organized activity in the EEG signal such as evoked responses or eye blinks results in synchronization and thus a drastic reduction in entropy. Although the contribution of eye blinks to the online-analysed EEG signal was minimized by the spatial filter approach, we ensured that no periods containing eye-blinks distorted the classification of desynchronization states. To this end, pupil data was read out in real-time and whenever a blink was detected by the eye tracker or pupil size was close to zero, a "mute" window of 1 second was initiated where incoming data were not considered further. EEG signals immediately following a blink thus were excluded from both, entering the desynchronization distribution and being classified as a high or low state.

Whenever a high or low state was detected, a new trial started with the presentation of a pure tone after which the response screen was shown and participants gave their response. Note that each tone was presented equally often during high and low states (30 times, yielding 210 trials per state, or 420 trials in total).

Pre-processing of pupil data: First, the inbuilt detection algorithm was used to locate blinks and saccades before pupil data were aligned with EEG recordings. Second, signal around blinks was interpolated using a cubic spline before low-pass filtering below 20 Hz and down-sampling to 50 Hz. Third, data were split up into trials (-2.5–3 seconds peristimulus). Finally, single trial time-courses of pupil size were visually inspected and noisy trials (1.3% ± 1.6%) were removed. For visualization purposes, pupil signals were expressed in percentage of the pre-stimulus maximum within a participant (-.5–0 s peristimulus). Un-transformed pupil data was used as a predictor in brain-brain as well as brain-behaviour models. Due to technical difficulties, data from one subject had to be excluded from further analyses.

EEG offline pre-processing: EEG pre-processing and analyses were carried out using the Fieldtrip and EEGLAB toolboxes [70,74] as well as custom code in Matlab® 2017a. First, and as a preparation for independent component analysis (ICA) only, data were re-referenced to the average of all channels, bandpass filtered between 1 and 100 Hz, subsequently down-sampled to 300 Hz, and split up into 2 seconds long epochs. Rare events like breaks between experimental blocks and noisy channels were excluded based on visual inspection. Second, data were decomposed into independent components using EEGLAB's runica algorithm. Visual inspection of topographies, time-courses, power spectra, and fitted dipoles (dipfit extension) was used to reject artefactual components representing eye blinks, lateral eye movements, heart rate,

muscle and electrode noise. Third, raw, un-processed data were loaded, previously detected noisy channels were removed and data were re-referenced to the average of all channels. ICA weights of non-artefactual components were applied to those data before excluded channels were interpolated. Finally, ICA-cleaned data were band-pass filtered between .5 and 100 Hz using a zero-phase finite impulse response filter and subsequently epoched between -2.5 and 3 seconds peristimulus. Single trials were visually inspected and rejected in case of excessive noise. On average 1 channel (±1 channel, M ± SD), 68.9% (± 7%) of all components, and1.4% (± 1.6%) of all trials were rejected.

EEG time–frequency domain analyses: Single trial complex-valued Fourier representations of the data were obtained through the convolution of cleaned and spatially filtered time-courses with frequency adaptive Hann-tapers (4 cycles) with a time-resolution of 100 Hz. Power from 1 to 40 Hz (in .5 Hz steps) and from 40 to 70 Hz (14 exponentially increasing steps) was calculated by squaring the modulus of the Fourier spectrum and was expressed as change in Decibel (dB) relative to average power in a baseline period (-1 to 0 s peristimulus).

Additionally, we calculated inter-trial phase coherence (ITC; $0 \leq ITC \geq 1$) and thus divided Fourier representations by their magnitude and averaged across trials before computing the magnitude of the average complex value. Importantly, since, ITC is only defined for a set of multiple trials but not for single trials, we computed the single-trial measure of jackknife-ITC (jITC[54,75]). In short, jITC of one trial is defined as the ITC of all trials but the one in question. Note that a trial highly phase-coherent with all others will result in a relatively low value of jITC, reversing the intuitive interpretation of ITC. In the remainder of this paper, we will thus use the term *single-trial phase coherence* when referring to 1–jITC.

Control analyses: To test the topographical specificity of EEG entropy, we averaged the re-referenced but otherwise raw EEG signal over seven visuo-occipital channels (PO3, PO4, PO7, PO8, POz, O1, O2). Note that this average of a channel selection (all seven visuo-occipital channels receiving equal weight in the average, while other channels effectively received weight 0) is conceptually not different from the way the more sophisticated, pilot–experiment-based auditory spatial filter was calculated. Subsequently, we calculated EEG entropy of this occipital cluster in the exact same way outlined above for auditory cortical areas. The resulting entropy signal was used to repeat all analyses of stimulus-related activity and behaviour. Precisely, mixed models of ITC, stimulus-related power and behaviour were re-run with visuo-cortical entropy. The performance of those models was evaluated by comparing them to the models based on auditory cortical entropy.

<u>*Statistical analyses*</u>

General approach: Trial-wise brain-behaviour and brain-brain relationships were analysed using (generalized) linear mixed-effects models (see below). We used single trial estimates of pre- and post-stimulus brain activity as well as binary decisions ("high vs. "low") as dependent variables. On the other hand, pre-stimulus entropy and pupil size served as predictors. To allow for an illustrative presentation of single subject data, dependent variables were binned based on predictor variables (see Fig. 3). Importantly, binning was used for visualization only and was not part of any statistical analyses reported here. Note, however, that single subject fits across bins

(of varying number; varying the number of bins between 3 and 7) qualitatively replicated effects of single-trial models.

Brain–behaviour relationships: As the main interest of this study lay in the influence of pre-stimulus desynchronization and pupil-linked arousal on perceptual sensitivity and response criterion, we combined a generalized linear-mixed-effects model approach with psychophysical modelling: single trial responses (high vs. low) of all participants were modelled as a logistic regression in R[76] using the lme4 package[77] and a logit link function. The main predictors used in the model were (1) the normalized pitch of presented tones (with respect to the median frequency, 7 levels), (2) pre-stimulus entropy (averaged between -.2 and 0 s peristimulus) and (3) pre-stimulus pupil size (averaged between -.5 and 0 s peristimulus). Pre-stimulus entropy and pupil size entered the model as both linear and quadratic predictors allowing us to test for non-linear relationships. We additionally included baseline entropy of each trial (3 seconds pre-stimulus) as a covariate to account for slow fluctuations in average entropy across the duration of the experiment. Note that such an approach is not only in line with current recommendations in statistical literature[78] but also comparable to the common inclusion of polynomials in models of functional imaging data[79]. To control for the influence of task duration, trial number was added as a regressor of no interest. Note that, in the resulting model, a main effect of pitch corresponds to the presence of psychometric response behaviour itself (probability of "high" responses across pitch levels), a main effect of another predictor (e.g. pupil size) represents a shift in response criterion, and an interaction of pitch and another predictor depicts a change in the slope of the psychometric function, i.e. a change in sensitivity.

Response times were measured relative to the offset of the presented tone and analysed irrespective of response outcome (correct vs. incorrect). To eliminate the impact of outliers, response times below .2 and above 2 seconds were excluded from further analyses[80]. Effects of pre-stimulus desynchronization and arousal on response speed (the inverse of response time, measured in 1/s) were analysed within a linear mixed-effect model framework. Hence, single-trial measures of response speed across all participants were considered as the dependent variable. This analysis approach allowed us to control for a number of other variables including trial number and task ease by adding them as regressors to the model.

Brain–brain relationships: To test the relationships between neural desynchronization and pupil-linked arousal with ongoing brain activity as well as auditory evoked responses we followed an analogous approach. Namely, different linear mixed-effects models with pre-stimulus entropy and pupil size as predictors were fitted for (i) pre-stimulus low (1–8 Hz) and (i) high (40–70 Hz) frequency power as proxies of ongoing activity. Similarly, different models were fitted for (i) post-stimulus (0–250 ms) single-trial phase coherence (1–8 Hz), as well as (ii) low and (iii) high frequency total power as measures of auditory evoked activity and stimulus processing (see Fig. 2A). Of note no other covariates than baseline entropy used to model brain–behaviour relationships were included since none explained any additional variance.

Model fitting: We employed an iterative model fitting procedure, starting with an intercept-only model, to arrive at the best fitting model[81,82].

Fixed effects were added to the model one at a time and the change in model fit was assessed using maximum likelihood estimation. An analogous procedure was adopted for random effects after the best fitting fixed-effect-only model had been

determined. We re-coded single trial pitch by first subtracting the median pitch and subsequently dividing by the new maximum, resulting in –1 and 1 for lowest and highest pitch, respectively, and 0 as the midpoint. We z-scored all continuous dependent variables across participants. In the case of binary response behaviour we used generalized linear mixed-effects models with a logit link function. For all other models we employed linear mixed-effects as distributions of dependent variables were not found to be significantly different from a normal distribution (all Shapiro–Wilk *P* values > .1). *P* values for individual model terms were derived using the Wald z-as-t procedure[83]. As a measure of effect size we report log odds ratio (log OR) for models of binary response behaviour end regression coefficients β for all other models alongside their respective standard errors (SE). A log OR of 0 indicates no effect for the regressor under consideration. Bayes factors (BF) were calculated for the comparison of two models with an equal number of terms that differed only in one predictor.

To additionally offer an intuitive comparison of predictors' effects on behavior we directly tested the difference of model estimates using a Wald test. In short, the Wald statistic puts the difference between two estimates from the same model in relation to the standard error of that difference. The resulting test statistic Z (Bolker et al., 2009) can be used to test the null hypothesis of no difference between the two estimates in a respective linear model. Z-values above or below ±1.96 denote $p<.05$.

To evaluate the performance of the real-time desynchronization detection algorithm described above, we re-calculated entropy (WPE) in the spatially filtered, un-cleaned EEG signal to then compute subject-wise averages of entropy time-courses for high state and low state trials, respectively. A series of paired t-test was used to examine state differences across time. We adjusted p-values to control for the false discovery rate[84].

Data availability: EEG data and pupillometry data will be made publicly available on the Open Science Framework (OSF) upon publication

Code availability: Custom computer code to reproduce all essential findings will be made publicly available on OSF upon publication.

1. Lee, T. H. *et al.* Arousal increases neural gain via the locus coeruleus-noradrenaline system in younger adults but not in older adults. *Nature Human Behaviour* **2**, 356–366 (2018).
2. McGinley, M. J. *et al.* Waking State: Rapid Variations Modulate Neural and Behavioral Responses. *Neuron* **87**, 1143–1161 (2015).
3. Pfeffer, T. *et al.* Catecholamines alter the intrinsic variability of cortical population activity and perception. *PLOS Biology* **16**, e2003453 (2018).
4. Curto, C., Sakata, S., Marguet, S., Itskov, V. & Harris, K. D. A simple model of cortical dynamics explains variability and state-dependence of sensory responses in urethane-anesthetized auditory cortex. *J. Neurosci.* **29**, 10600–10612 (2009).
5. Marguet, S. L. & Harris, K. D. State-Dependent Representation of Amplitude-Modulated Noise Stimuli in Rat Auditory Cortex. *Journal of Neuroscience* **31**, 6414–6420 (2011).
6. Pachitariu, M., Lyamzin, D. R., Sahani, M. & Lesica, N. a. State-dependent population coding in primary auditory cortex. *Journal of neuroscience* **35**, 2058–73 (2015).
7. Aston-Jones, G. & Cohen, J. D. An Integrative Theory of Locus Coeruleus-Norepinephrine Function: Adaptive Gain and Optimal Performance. *Annual Review of Neuroscience* **28**, 403–450 (2005).
8. Joshi, S., Li, Y., Kalwani, R. M. & Gold, J. I. Relationships between Pupil Diameter and Neuronal Activity in the Locus Coeruleus, Colliculi, and Cingulate Cortex. *Neuron* **89**, 221–234 (2016).
9. Reimer, J. *et al.* Pupil fluctuations track rapid changes in adrenergic and cholinergic activity in cortex. *Nature Communications* **7**, (2016).
10. Gelbard-Sagiv, H., Magidov, E., Sharon, H., Hendler, T. & Nir, Y. Noradrenaline Modulates Visual Perception and Late Visually Evoked Activity. *Current Biology* 1–11 (2018). doi:10.1016/j.cub.2018.05.051
11. McGinley, M. J., David, S. V. & McCormick, D. A. Cortical Membrane Potential Signature of Optimal States for Sensory Signal Detection. *Neuron* **87**, 179–192 (2015).
12. Murphy, P. R., Vandekerckhove, J. & Nieuwenhuis, S. Pupil-Linked Arousal Determines Variability in Perceptual Decision Making. *PLoS Computational Biology* **10**, (2014).
13. Yerkes, R. M. & Dodson, J. D. The relation of strength of stimulus to rapidity of habit-formation. *Journal of Comparative Neurology and Psychology* **18**, 459–482 (1908).
14. Faller, J., Cummings, J., Saproo, S. & Sajda, P. Regulation of arousal via online neurofeedback improves human performance in a demanding sensory-motor task. *PNAS* 201817207 (2019). doi:10.1073/pnas.1817207116
15. van den Brink, R. L., Murphy, P. R. & Nieuwenhuis, S. Pupil Diameter Tracks Lapses of Attention. *PLoS ONE* **11**, e0165274 (2016).
16. Neske, G. T. & McCormick, D. A. Distinct waking states for strong evoked responses in primary visual cortex and optimal visual detection performance. *bioRxiv* (2018). doi:10.1101/437681
17. Beaman, C. B., Eagleman, S. L. & Dragoi, V. Sensory coding accuracy and perceptual performance are improved during the desynchronized cortical state. *Nature communications* **8**, 1308 (2017).
18. Goard, M. & Dan, Y. Basal forebrain activation enhances cortical coding of natural scenes. *Nature Neuroscience* **12**, 1444–1449 (2009).
19. Pinto, L. *et al.* Fast modulation of visual perception by basal forebrain cholinergic neurons. *Nature Neuroscience* **16**, 1857–1863 (2013).
20. Sakata, S. State-dependent and cell type-specific temporal processing in auditory thalamocortical circuit. *Scientific reports* **6**, 18873 (2016).

21. Haider, B., Häusser, M. & Carandini, M. Inhibition dominates sensory responses in the awake cortex. *Nature* **493**, 97–100 (2012).
22. Renart, A. *et al.* The asynchronous state in cortical circuits. *Science (New York, N.Y.)* **327**, 587–90 (2010).
23. Speed, A., Del Rosario, J., Burgess, C. P. & Haider, B. Cortical State Fluctuations across Layers of V1 during Visual Spatial Perception. *Cell Reports* **26**, 2868-2874.e3 (2019).
24. Vinck, M., Batista-Brito, R., Knoblich, U. & Cardin, J. A. Arousal and Locomotion Make Distinct Contributions to Cortical Activity Patterns and Visual Encoding. *Neuron* **86**, 740–754 (2015).
25. Okun, M., Steinmetz, N. A., Lak, A., Dervinis, M. & Harris, K. D. Distinct structure of cortical population activity on fast and infraslow timescales. *bioRxiv* (2018). doi:10.1093/cercor/bhz023
26. Harris, K. D. & Thiele, A. Cortical state and attention. *Nature Reviews Neuroscience* **12**, 509–523 (2011).
27. Fadlallah, B., Chen, B., Keil, A. & Príncipe, J. Weighted-permutation entropy: A complexity measure for time series incorporating amplitude information. *Physical Review E* **87**, 022911 (2013).
28. Waschke, L., Wöstmann, M. & Obleser, J. States and traits of neural irregularity in the age-varying human brain. *Scientific Reports* **7**, 17381 (2017).
29. Sarasso, S. *et al.* Consciousness and complexity during unresponsiveness induced by propofol, xenon, and ketamine. *Current Biology* **25**, 3099–3105 (2015).
30. Gao, R., Peterson, E. J. & Voytek, B. Inferring synaptic excitation/inhibition balance from field potentials. *NeuroImage* **158**, 70–78 (2017).
31. Jazayeri, M. & Afraz, A. Navigating the Neural Space in Search of the Neural Code. *Neuron* **93**, 1003–1014 (2017).
32. Ezzyat, Y. *et al.* Closed-loop stimulation of temporal cortex rescues functional networks and improves memory. *Nature Communications* **9**, (2018).
33. Sitaram, R. *et al.* Closed-loop brain training: the science of neurofeedback. *Nature Neuroscience* (2016). doi:10.1038/nrn.2016.164
34. Robbins, T. W. Arousal systems and attentional processes. *Biological Psychology* **45**, 57–71 (1997).
35. Carter, M. E. *et al.* Tuning arousal with optogenetic modulation of locus coeruleus neurons. *Nat Neurosci* **13**, 1526–1533 (2010).
36. Herrmann, B., Maess, B. & Johnsrude, I. S. Aging Affects Adaptation to Sound-Level Statistics in Human Auditory Cortex. *The Journal of Neuroscience* 1489–17 (2018). doi:10.1523/JNEUROSCI.1489-17.2018
37. de Cheveigne, A. & Simon, J. Z. Denoising based on spatial filtering. *Journal of Neuroscience Methods* **171**, 331–339 (2008).
38. Reimer, J. *et al.* Pupil Fluctuations Track Fast Switching of Cortical States during Quiet Wakefulness. *Neuron* **84**, 355–362 (2014).
39. Makeig, S., Debener, S., Onton, J. & Delorme, A. Mining event-related brain dynamics. *Trends in Cognitive Sciences* **8**, 204–210 (2004).
40. Tallon-Baudry, C., Bertrand, O., Delpuech, C. & Pernier, J. Stimulus Specificity of Phase-Locked and Non-Phase-Locked 40 Hz Visual Responses in Human. *J. Neurosci.* **16**, 4240–4249 (1996).
41. Tiitinen, H. T. *et al.* Selective attention enhances the auditory 40-Hz transient response in humans. *Nature* **364**, 59–60 (1993).
42. Peixoto, D. *et al. Decoding and perturbing decision states in real time.* (Neuroscience, 2019). doi:10.1101/681783
43. de Gee, J. W. *et al.* Dynamic modulation of decision biases by brainstem arousal systems. *eLife* **6**, (2017).

44. Pakan, J. M. *et al.* Behavioral-state modulation of inhibition is context-dependent and cell type specific in mouse visual cortex. *eLife* **5**, (2016).
45. Shimaoka, D., Harris, K. D. & Carandini, M. Effects of Arousal on Mouse Sensory Cortex Depend on Modality. *Cell Reports* **22**, 3160–3167 (2018).
46. Zagha, E., Casale, A. E., Sachdev, R. N. S., McGinley, M. J. & McCormick, D. A. Motor Cortex Feedback Influences Sensory Processing by Modulating Network State. *Neuron* **79**, 567–578 (2013).
47. Zagha, E. & McCormick, D. A. Neural control of brain state. *Current Opinion in Neurobiology* **29**, 178–186 (2014).
48. Cohen, M. R. & Maunsell, J. H. R. Attention improves performance primarily by reducing interneuronal correlations. *Nature Neuroscience* **12**, 1594–1600 (2009).
49. Cohen, M. R. & Maunsell, J. H. R. Using Neuronal Populations to Study the Mechanisms Underlying Spatial and Feature Attention. *Neuron* **70**, 1192–1204 (2011).
50. Nandy, A., Nassi, J. J., Jadi, M. P. & Reynolds, J. Optogenetically induced low-frequency correlations impair perception. *eLife* **8**, (2019).
51. Kayser, S. J., McNair, S. W. & Kayser, C. Prestimulus influences on auditory perception from sensory representations and decision processes. *Proceedings of the National Academy of Sciences* **113**, 201524087 (2016).
52. Iemi, L., Chaumon, M., Crouzet, S. M. & Busch, N. A. Spontaneous Neural Oscillations Bias Perception by Modulating Baseline Excitability. *The Journal of Neuroscience* **37**, 807–819 (2017).
53. Samaha, J., Iemi, L. & Postle, B. R. Prestimulus alpha-band power biases visual discrimination confidence, but not accuracy. *Consciousness and Cognition* **54**, 47–55 (2017).
54. Wöstmann, M., Waschke, L. & Obleser, J. Prestimulus neural alpha power predicts confidence in discriminating identical auditory stimuli. *European Journal of Neuroscience* 285577 (2018). doi:10.1111/ejn.14226
55. Kloosterman, N. A. *et al.* Humans strategically shift decision bias by flexibly adjusting sensory evidence accumulation. *eLife* **8**, e37321 (2019).
56. Rajagovindan, R. & Ding, M. From Prestimulus Alpha Oscillation to Visual-evoked Response: An Inverted-U Function and Its Attentional Modulation. *Journal of Cognitive Neuroscience* **23**, 1379–1394 (2011).
57. Sauseng, P. *et al.* Are event-related potential components generated by phase resetting of brain oscillations? A critical discussion. *Neuroscience* **146**, 1435–1444 (2007).
58. Shah, A. S. *et al.* Neural Dynamics and the Fundamental Mechanisms of Event-related Brain Potentials. *Cerebral Cortex* **14**, 476–483 (2004).
59. Tallon-Baudry, C. & Bertrand, O. Oscillatory gamma activity in humans and its role in object representation. *Trends in Cognitive Sciences* **3**, 12 (1999).
60. Voigt, M. B., Yusuf, P. A. & Kral, A. Intracortical Microstimulation Modulates Cortical Induced Responses. *The Journal of Neuroscience* **38**, 7774–7786 (2018).
61. Morillon, B., Hackett, T. A., Kajikawa, Y. & Schroeder, C. E. Predictive motor control of sensory dynamics in auditory active sensing. *Current Opinion in Neurobiology* **31**, 230–238 (2015).
62. Otazu, G. H., Tai, L.-H., Yang, Y. & Zador, A. M. Engaging in an auditory task suppresses responses in auditory cortex. *Nature Neuroscience* **12**, 646–654 (2009).
63. Arieli, A., Sterkin, A., Grinvald, A. & Aertsen, A. Dynamics of ongoing activity: explanation of the large variability in evoked cortical responses. *Science (New York, N.Y.)* **273**, 1868–1871 (1996).
64. Schölvinck, M. L., Saleem, A. B., Benucci, A., Harris, K. D. & Carandini, M. Cortical state determines global variability and correlations in visual cortex. *The Journal of Neuroscience* **35**, 170–8 (2015).

65. Lin, I.-C., Okun, M., Carandini, M. & Harris, K. D. The Nature of Shared Cortical Variability. *Neuron* **87**, 644–656 (2015).
66. Mather, M., Clewett, D., Sakaki, M. & Harley, C. W. Norepinephrine ignites local hotspots of neuronal excitation: How arousal amplifies selectivity in perception and memory. *Behavioral and Brain Sciences* **39**, (2016).
67. Johnson, D. M. Generalization of a reference scale for judging pitch. *Journal of Experimental Psychology* **39**, 316–321 (1949).
68. Kothe, C. Lab Streaming Layer. (2014). Available at: https://code.google.com/archive/p/labstreaminglayer/.
69. Herrmann, B., Maess, B. & Johnsrude, I. S. Aging Affects Adaptation to Sound-Level Statistics in Human Auditory Cortex. *The Journal of Neuroscience* 1489–17 (2018). doi:10.1523/JNEUROSCI.1489-17.2018
70. Oostenveld, R., Fries, P., Maris, E. & Schoffelen, J.-M. FieldTrip: Open source software for advanced analysis of MEG, EEG, and invasive electrophysiological data. *Computational intelligence and neuroscience* **2011**, 156869 (2011).
71. Pascual-Marqui, R. D. Standardized low-resolution brain electromagnetic tomography (sLORETA): technical details. *Methods and findings in experimental and clinical pharmacology* **24 Suppl D**, 5–12 (2002).
72. Bandt, C. & Pompe, B. Permutation entropy: a natural complexity measure for time series. *Physical review letters* **88**, 174102 (2002).
73. Riedl, M., Müller, A. & Wessel, N. Practical considerations of permutation entropy: A tutorial review. *European Physical Journal: Special Topics* **222**, 249–262 (2013).
74. Delorme, A. & Makeig, S. EEGLAB: an open source toolbox for analysis of single-trial EEG dynamics including independent component analysis. *Journal of Neuroscience Methods* **134**, 9–21 (2004).
75. Richter, C. G., Thompson, W. H., Bosman, C. A. & Fries, P. A jackknife approach to quantifying single-trial correlation between covariance-based metrics undefined on a single-trial basis. *NeuroImage* **114**, 57–70 (2015).
76. R Core Team. R: A Language and Environment for Statistical Computing. (2018).
77. Bates, D., Mächler, M., Bolker, B. & Walker, S. Fitting Linear Mixed-Effects Models Using lme4. *Journal of Statistical Software* **67**, 251–264 (2015).
78. Senn, S. Change from baseline and analysis of covariance revisited. *Statist. Med.* **25**, 4334–4344 (2006).
79. Kay, K. N., David, S. V., Prenger, R. J., Hansen, K. A. & Gallant, J. L. Modeling low-frequency fluctuation and hemodynamic response timecourse in event-related fMRI. *Hum. Brain Mapp.* **29**, 142–156 (2008).
80. Ratcliff, R. Methods for dealing with RT outliers. *Psychological Bulletin* **114**, 510–532 (1993).
81. Tune, S., Wöstmann, M. & Obleser, J. Probing the limits of alpha power lateralisation as a neural marker of selective attention in middle-aged and older listeners. *European Journal of Neuroscience* **48**, 2537–2550 (2018).
82. Alavash, M., Tune, S. & Obleser, J. Modular reconfiguration of an auditory-control brain network supports adaptive listening behavior. *bioRxiv* 409797 (2018). doi:10.1101/409797
83. Luke, S. G. Evaluating significance in linear mixed-effects models in R. *Behavior Research Methods* **49**, 1494–1502 (2017).
84. Benjamini, Y. & Hochberg, Y. Controlling the false discovery rate: a practical and powerful approach to multiple testing. *Journal of the Royal Statistical Society B* **57**, 289–300 (1995).